

SCOPING STUDY ON COASTAL SQUEEZE IN THE AYEYARWADY DELTA

M.E.N. KROON⁽¹⁾, J. RIP⁽²⁾, M.M. RUTTEN⁽³⁾, M. J. F. STIVE⁽⁴⁾ and SAI WUNNA⁽⁵⁾

⁽¹⁾ Delft University of Technology, Delft, The Netherlands,
m.e.n.kroon@student.tudelft.nl

⁽²⁾ Delft University of Technology, Delft, The Netherlands,
j.rip@student.tudelft.nl

⁽³⁾ Delft University of Technology, Delft, The Netherlands,
m.m.rutten@tudelft.nl

⁽⁴⁾ Delft University of Technology, Delft, The Netherlands,
m.j.f.stive@tudelft.nl

⁽⁵⁾ Irrigation Technology Center, Bago, Myanmar,
saiwunna1975@gmail.com

ABSTRACT

Coastal squeeze is the reduction in the space of coastal habitats to operate (Phan et al, 2014) and an important cause for coastline retreat, increase in flood risk, salinity intrusion etc. Land use changes, such as deforestation and urbanization, reduce the space of natural habitats, such as mangrove forests, and cause deterioration of these habitats, that leads to reduction of their natural protective and provisioning functions. Costs related to these function losses can be avoided by early recognition of coastal squeeze and early action. In this research we investigate how remote sensing imagery data can contribute to early recognition of coastal squeeze.

The case study is the lower Ayeyarwady delta in Myanmar, a crucial agricultural zone nicknamed the 'Ricebowl of Myanmar'. The coastal zone in Myanmar is subject to climate change, urbanization, extreme weather conditions (cyclones), increase in agri- and aquaculture and (illegal) felling of mangrove. This has already led to large loss of biodiversity and increased flood risk.

Remote sensing analysis based on LANDSAT imagery has been done in attempt to identify land use and coastline change.

Keywords: coastal squeeze, land use, classification, QGIS, ground truthing

1. INTRODUCTION

1.1 Problem definition

The coastal zone in Myanmar is increasingly in danger because of sea level rise, urbanization, (illegal) felling of mangrove, aquaculture, agriculture and infrastructural development. The space for natural coastal processes reduces, is squeezed. In many coastal areas in the world, coastal squeeze has led to large loss of biodiversity and increased flood risk (Phan et al, 2014). In retrospect, these problems could have been avoided to a large extent by actions such as more careful spatial planning, mangrove conservation and "Building with Nature" (Waterman, 1995).

The term Coastal Squeeze started appearing in literature around 2003. The following definition has been distilled from the article 'Coastal squeeze in a historical perspective' (Doody, 2004); "Coastal development such as urbanization, agriculture, aquaculture and infrastructure play a role as blocking barrier, this stops the migration of the coastal ecosystems which tend to retreat landward when relative sea level is rising. This leads to the loss of valuable coastal habitats".

Figure 1 presents the forcing factors that are suspected to cause coastal squeeze. Physical forcing factors are the influence of the tide, sediment transport (along the coast and the supply from rivers), extreme events such as storm surges, river discharges and land subsidence. Socio-economics forcing factors influence the land use in the coastal area. Land use changes consist for example of the felling of mangrove forests, or an increase in the areas used for agriculture. Salinity intrusion plays a role in the possibilities of land use, e.g. in saline areas paddy fields can only produce crops during the monsoon season. Also in the context of socio economic forcing land subsidence can be addressed, due to ground water extraction for drinking water and irrigation purposes.

This paper addresses one of the possible signs for coastal squeeze, namely the relation between on one hand coastline retreat and on the other hand land use changes in the Ayeyarwady delta. The forcing factors will be described in more detail in Sections 1.1.2 and 1.1.3.

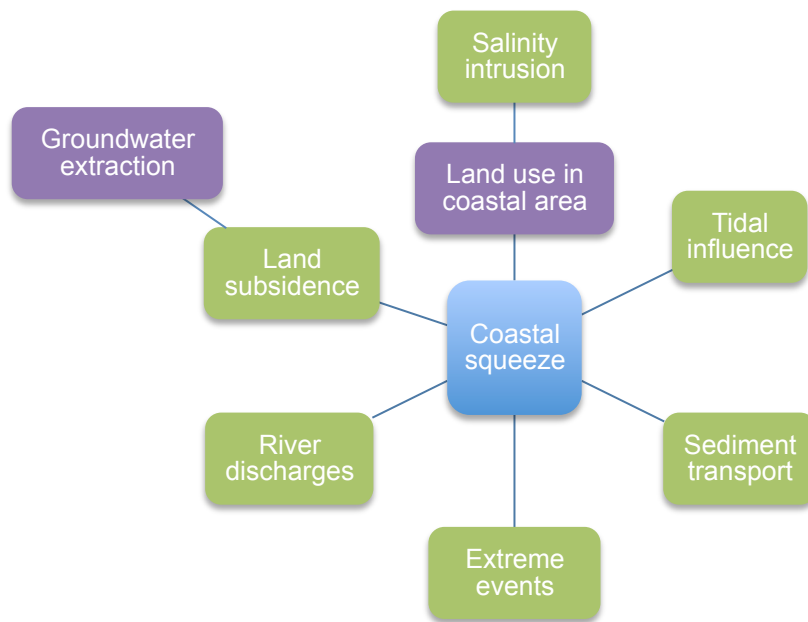


Figure 1. Forcings that are suspected to cause coastal squeeze. Items in green boxes represent physical forcings, in purple boxes socio-economic forcings.

1.1.1 Research area

The Ayeyarwady delta is located in the midst of the Myanmar coastline. Here the Ayeyarwady River enters the Gulf of Andaman. The delta is fringed by the Andaman gulf, with a semi diurnal tide and a mean tidal range in the mouths of the Ayeyarwady river between 2 and 4 meter (Ramaswamy, 2008). It is classified as a mud-silt tide-dominated system (Hedley, 2010).

The area of the delta that is particularly focused on in this paper is the area that is affected by salt intrusion. This area is shown in Figure 2. The highlighted area indicates the average salinity intrusion in March; this is at the end of the dry season when salinity is highest and measured during spring tide.¹ The salinity criterion is 1 PPT at 1 m water depth.



Figure 2. Location of research area

¹ This line is based on salinity measurements conducted by the Hydrology Branch of Irrigation Department. The data used to interpolate in order to draw this line is of 2013 and 2014. Measurements before are existent but locations were not measured by GPS until 2013.

1.1.2 Physical forcing factors

The Ayeyarwady delta is subject to numerous physical processes affecting the area. A shortlist of these factors which are of influence on the land use and coastline position is indicated in Figure 1. In all these processes the lack of accurate and trustworthy data leads to rough estimations and large uncertainty factors in literature (Furuichi, 2009; Ramaswamy, 2008; Hedley, 2010).

For a long time it was believed that the Ayeyarwady Delta was prograding with 2,5 km into the Andaman Sea every 100 years. This was derived from papers written by Chhibber (1934), Rodolfo (1975) and Aung (2003). Hedley et al. (2010) challenged this belief, comparing actual coastline progradation rates over the past decades to this accretion number. Hedley et al. (2010) state that the delta currently hedis in an equilibrium state.

The Ayeyarwady River has an estimated annual mean discharge of $379 \times 10^9 \text{ m}^3$, discharging up to $90 \times 10^9 \text{ m}^3/\text{month}$ during monsoon season (Furuichi et al, 2009).

There is large potential in the development of hydropower in Myanmar. Mainly in the upstream mountainous regions. Damming can have a large influence on sediment transport, as can be seen in the decrease of sediment concentration in the Yangtze and Yellow river over the last decades (Walling, 2006) But, as research from Furuichi et al.(2009) shows, the main source of sediment in the delta is the Central Dry Zone in the middle of Myanmar, including the catchment of the Chindwin. Quantities cannot be given due to lack of data. This suggests that although many plans are made for hydropower which will have large (local) environmental impact, the impact on sediment feeding to the Delta is expected to be limited.

Most of the muddy sediment that is deposited at the coast is redistributed and brought to the nearby Gulf of Martaban by the south west monsoon (Rodolfo, 1975).

Cyclone Nargis hit the Ayeyarwady Delta in May 2008. It caused over one hundred thousand casualties as well as approximately 2 million people were displaced. For the natural environment, the cyclone carried very large amounts of rain and an exceptional high surge level into the delta. This caused the delta to flood up to 50 km land inwards, with surge levels as high as +7 m MSL. (Fritz, 2009) This event still has very large consequences today for the use of certain land because of saline contamination and decreased yields of cropland. Furthermore Nargis destroyed large parts of mangrove forests and changed the position of the coastline (Fritz, 2009). Nargis was by far the most severe cyclone in recent history hitting the delta.

1.1.3 Socio-economic forcings

The Ayeyarwady delta is home to the largest mangrove forest of the country, but also suffers from the highest deforestation rate in the country (Webb et al, 2013). This mangrove forest supports vital resources like fuel wood and in-shore fishing industries. It is also very important for coastline protection against storm surges, which became very clear after cyclone Nargis (Fritz, 2009).

The delta has a dense population approximating 7.7 million people in 2007(Webb et al, 2013). In 2014 a recount of the population has been done, the number then was rescaled to 6.2 million inhabitants of Ayeyarwady region. Despite this decrease in amount, the population density is the third highest of all states/regions (United Nations, 2014). This puts large pressure on the use of land, mainly because of agricultural expansion. This, together with fuelwood extraction, leads to mangrove deforestation.

Reforestation projects have been initiated for the last 20 years by several Non Governmental Organisations and the Forestry Department. Still the region sighs under increased cultivation of the area to paddy land in order to supply rice for the lower Myanmar regions (Webb et al, 2013). In order to prevent flooding and salt intrusion large-scale embankments, sluices and drainage systems have been constructed(Delta Alliance, 2013). These rigid structures interact with the environment, creating hydrological boundaries and thus squeeze the coastal habitat..

2. METHODOLOGY

2.1 Land use classification

2.1.1 Image acquisition

Landsat 5 and 7 images of path 133 and row 49 from the Climate Data Record(CDR) database of the United States Geological Survey(USGS) of are used for this research. These images contain atmospherically corrected surface reflectance data, and are accompanied by a mask layer for clouds and their shadows. Pixels labelled as cloud or shadow were removed from the image. For each year that is analysed a 'master' Landsat image is chosen, preferably around the month December of that year (because our ground truthing took place in that month) and with as little cloud cover as possible. However, these images can still have data gaps because of cloud & shadow contamination and Scan Line Corrector(SLC)-off gaps (images after 2003). Therefore a mosaicking tool is used to replace empty pixels for each band of the master images with valid pixels from other images from the same year, following the methodology from the Web-Enabled Landsat Data (WELD) project (Roy et al, 2014). An overview of the master images and their potential substitutes is presented in Table 1. The master image has priority 1, and missing pixels are first filled with pixels from the priority 2 image, and then with pixels from the priority 3 image.

Table 1. Overview of used Landsat 5 and 7 images for this research.

Year	Satellite	Priority	Image date
2014	Landsat 7	1	23-12-14
		2	07-12-14
		3	21-11-14
2010	Landsat 7	1	10-11-10
		2	25-10-10
		3	16-04-10
2008 (before Nargis)	Landsat 7	1	06-02-08
		2	22-02-08
		3	21-01-08
2008 (after Nargis)	Landsat 7	1	22-12-08
		2	06-12-08
		3	20-11-08
2005	Landsat 7	1	30-12-05
		2	12-11-05
		3	11-10-05
2000	Landsat 7	1	31-01-00
1989	Landsat 5	1	01-02-89

2.1.2 Ground truthing

Using Normalized Difference Vegetation Index (NDVI) and colour composite maps (made with the Landsat bands) and an OpenStreetMaps road vector layer, regions of interest were identified. These are the regions that together contain a complete set of different types of land cover identified in the maps, and that are easily accessible (near a road). A Google Earth layer was also imported to visually determine regions of interest on the map with a larger resolution than the Landsat images. Within the regions of interest, areas of equal land use were measured by walking around them with a GPS tool (Samsung Galaxy S4 mini with ViewRanger application). For some areas (in particular with dense vegetation) it was not possible to walk around it, in order to track the full polygon with GPS. In these cases a point measurement was done (save the location as a GPS waypoint) and the polygon was later drawn by hand in QGIS with the help of a Google Earth layer, and the NDVI and colour composite maps. The classes 'Degraded mangrove' and 'Sediments' were not found during fieldwork, but some training polygons were constructed with help of Google Earth (following Weber et al (2014)). For the class other vegetation a large polygon on a mountain range was added in the same way.

The following land use classes are used in this research:

1. Water: Rivers and the sea.
2. Paddy field: Paddy fields have various spectral signatures depending on the growth stage. In this research no differentiation is made between these growth stages, therefore polygons of as many growth stages were collected during the fieldwork and they will be used to train the overall class 'paddy field'.
3. Mangrove: Mangrove forests are present near the coastline and rivers where there is salinity intrusion.
4. Degraded mangrove: Sparse mangrove forest, with patches of bare soil.
5. Other vegetation: Non-mangrove dense vegetation consists of orchards (e.g. snow apple, betel nut), plantations (e.g. banana, coconut, nypal) or natural dense vegetation, mainly alongside (fresh) rivers and creeks.
6. Urban areas: Urban areas consist of densely populated areas or more rural areas where also a lot of vegetation is present.
7. Sediments: Sandy/muddy sediment deposits along the coast and tidal rivers.

During fieldwork, small water bodies such as drinking water lakes, fishponds and ponds near monasteries were found. The area of these water bodies was small, usually less than five Landsat pixels. Also, in most cases dense vegetation was present around the boundaries of the water body, which was included in the area tracked with GPS. This distorts the true spectral signature, as this increases the reflection in the infrared spectrum. Due to the minimal amount of training pixels and the distortion in the spectral signatures, it was decided not to include this type of land use as a separate class. Table 2 gives a summary of the training data set.

Table 2. Summary of training data set

Class ID	Class	Pixels	Polygons
1	Water	12870	7

2	Paddy	1987	25
3	Mangrove	2259	8
4	Degraded Mangrove	1816	7
5	Other vegetation	8421	15
6	Urban	1554	7
7	Sediments	3179	6
Total		32086	75

2.1.3 Image classification

The first fieldwork took place between 15 and 17 December 2014. The second fieldwork took place on 5 January 2015. Therefore the Landsat 7 merged image of 2014 was used to create spectral signatures for each class (as this is the image that is closest to these dates). These spectral signatures are also used to classify images from other years, because we assume the spectral signatures of the land cover types will not have changed significantly over the years. The GRASS(Geographical Resources Analysis Support System, <http://grass.osgeo.org>) plugin in QGIS was used to create spectral signatures of each class and perform a Sequential Maximum A Posteriori (SMAP) classification. The classification was executed on the full Landsat tile.

In order to improve the classification, majority analysis with a kernel size of 3 pixels was applied to remove noise, as well as some masks:

1. Mangrove – land elevation. Mangrove can physically not exist at elevations exceeding 35 meters above sea level. Therefore, following Weber et al (2014), all pixels classified as mangrove at elevations above 35 meters are reclassified as 'Other vegetation'. ASTER Global Digital Elevation Model(GDEM) raster images (RMS-error accuracy between 10-25 m, spatial resolution of 30m) were used to assess the land elevation.
2. Pixels classified as sediments, which are not adjacent to water, are probably paddy fields. Empty (muddy) paddy fields can yield a similar spectral signature as sediments. Therefore a mask was made with areas that are at most 30 pixels (900 m) away from water. Pixels classified as sediments which are not within this mask, are reclassified as paddy.

2.2 Coastline Evolution

Detection of the change of coastline is done by analyzing Landsat satellite images, since 1978. Vectors of the coastlines are generated for all available years in order to obtain a comparable set of lines which can indicate progradation or retrogradation and its approximate speed.

First band 5 of the image (for Landsat 7 and older) is manipulated into a binary image; land and water. The threshold for every image was obtained visually since all images have a unique bandwidth of maximum and minimum values. After this the raster image is vectorized. This polygon is transformed to lines. These lines are simplified so only the lowest part of the delta remains. The lines obtained follow the outline of pixels, and are hence physically unrealistic. The lines are therefore smoothed. It was visually established that the Snakes method for line smoothing(Kass et al, 1988) gave overall the most reliable results, as can be seen in the example in Figure 3. However, the precision of the coastline position, considering a pixel size of 30 meters, has an inaccuracy in the order of 30-60 meters.

This method has been used to extract coastlines from years and Landsat images as stated in Table 3.

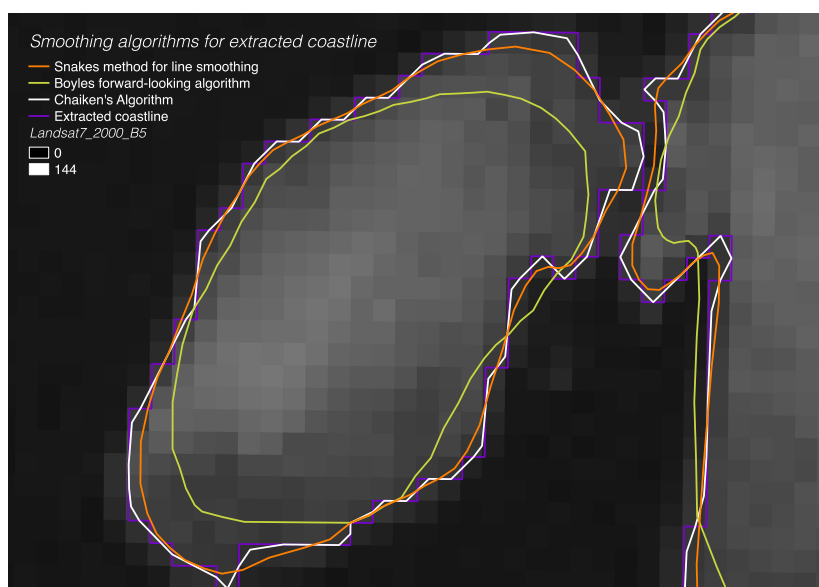


Figure 3. Zoom of coastline generation from Landsat 7 imagery with different smoothing algorithms

Table 3. Satellite images used for coastline extraction

Year	Image	Capture time
1974	1974_merge_nodatafill (own merging with Landsat 1 images)	03:25:19
1989	LT41330491989032XXX02_B4	03:34:44
2000	LE71330492000031SGS00_B5	03:54:53
2008 (Before Nargis)	See Table 1 – Band 5	03:52:10
2008 (After Nargis)	See Table 1 – Band 5	
2010	See Table 1 – Band 5	03:54:44
2014	LC81330492014317LGN00_B5	04:00:37

2.3 Auxiliary data

2.3.1 Salinity measurements

Water quality measurements have been done in the research area, using a CTD (conductivity, Temperature, Depth) meter. The salinity (PPT) measured is shown in Figure 4.

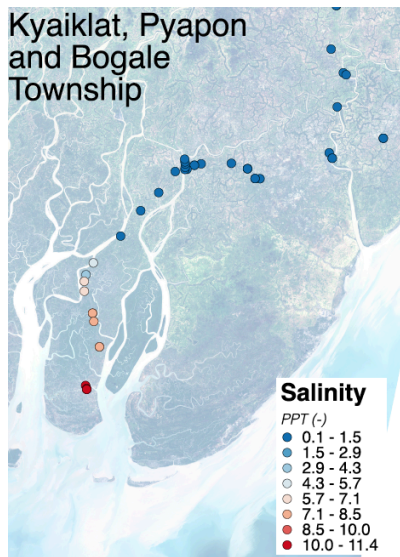


Figure 4. Result of salinity measurements with CTD

2.3.2 Analogue maps

In the case of a (hand drawn) map, extra preparation is needed to vectorize the coastline. First step is to georeference the TIFF file, in order to redefine all projections used in different maps. Two tools are used for this, depending on the approach of the georeferencing. This approach is determined by the projection of the map used and if it contains the longitude/latitude raster lines. When a map does not contain the raster lines and/or the latitude/longitude coordinate system, the map is visually georeferenced. When the map is drawn with raster lines of longitude/latitude type, the georeferencing can be done faster and more accurate, by defining the nodes of these lines and recalculate the projection to a general WGS 84 projection. This method has successfully been used for maps of 1941 and 1950. Part of these coastlines is shown on top of a Landsat 8 image of 2014 (Figure 5).

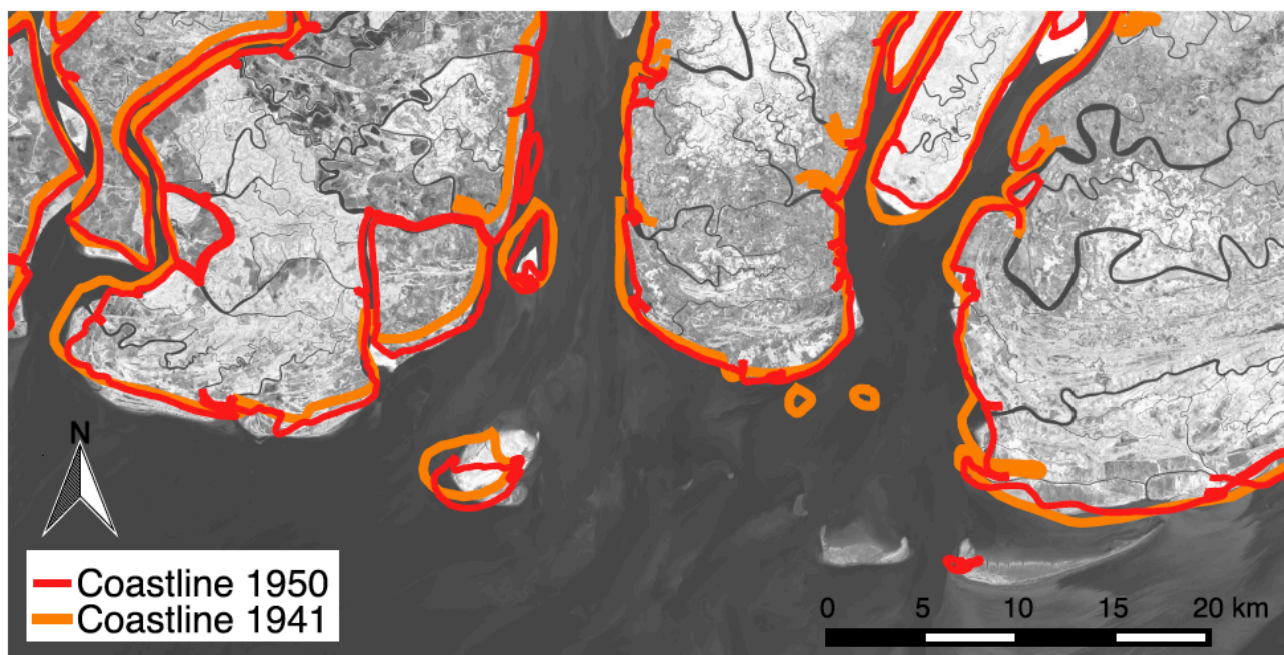


Figure 5. Coastlines from analogue maps of 1941 and 1950

3. RESULTS

3.1 Land use classification

Figure 6 presents the mean spectral signatures per class of the training data set, based on the merged 2014 image. It shows that the spectral signatures of classes mangrove and other vegetation are much alike, which was to be expected because they are both dense vegetation. The classes paddy, urban, degraded mangrove and sediments are also alike. The SMAP algorithm identified 5 subclasses within each class. Figure 7 shows that the subclasses within the class paddy are quite different. This is due to the different growth stages of the paddy fields.

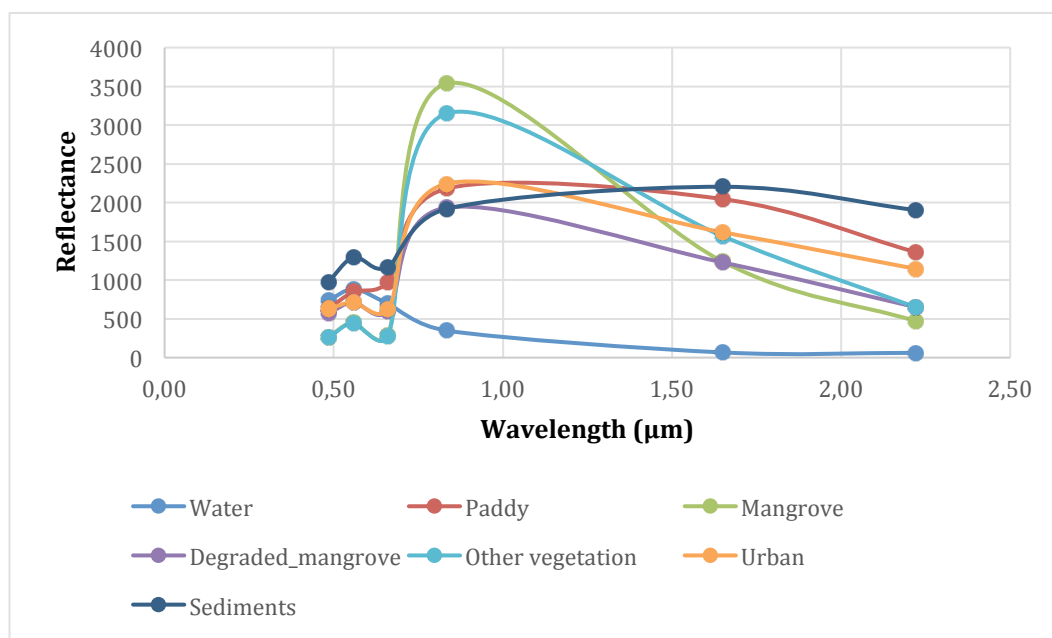


Figure 6. Mean spectral signature per class of the training data set, based on the merged 2014 image.

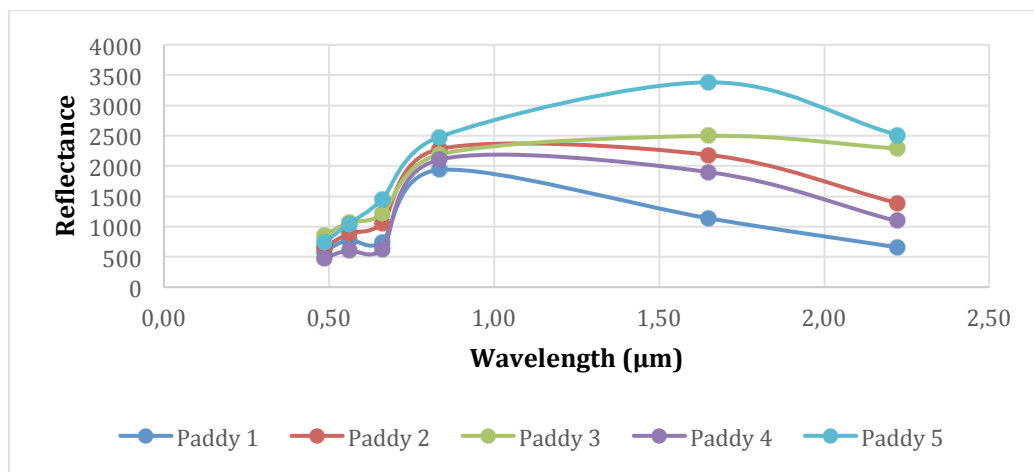


Figure 7. Mean spectral signature per subclass of the class paddy, based on the merged 2014 image.

Figure 8 presents the output of the land use classification on the 2014 image. There are 'stripes' visible in the image, because the SLC-off gaps were filled with pixels from other images than the master image (as explained before). The surface reflectance was not always the same on these other images, causing other classifications. Table 4 shows the areas of land use for the various years. The changes in area do not show an overall trend; the shifts in land use are caused by quality differences in the imagery or classification method, rather than resembling actual land use change over time.

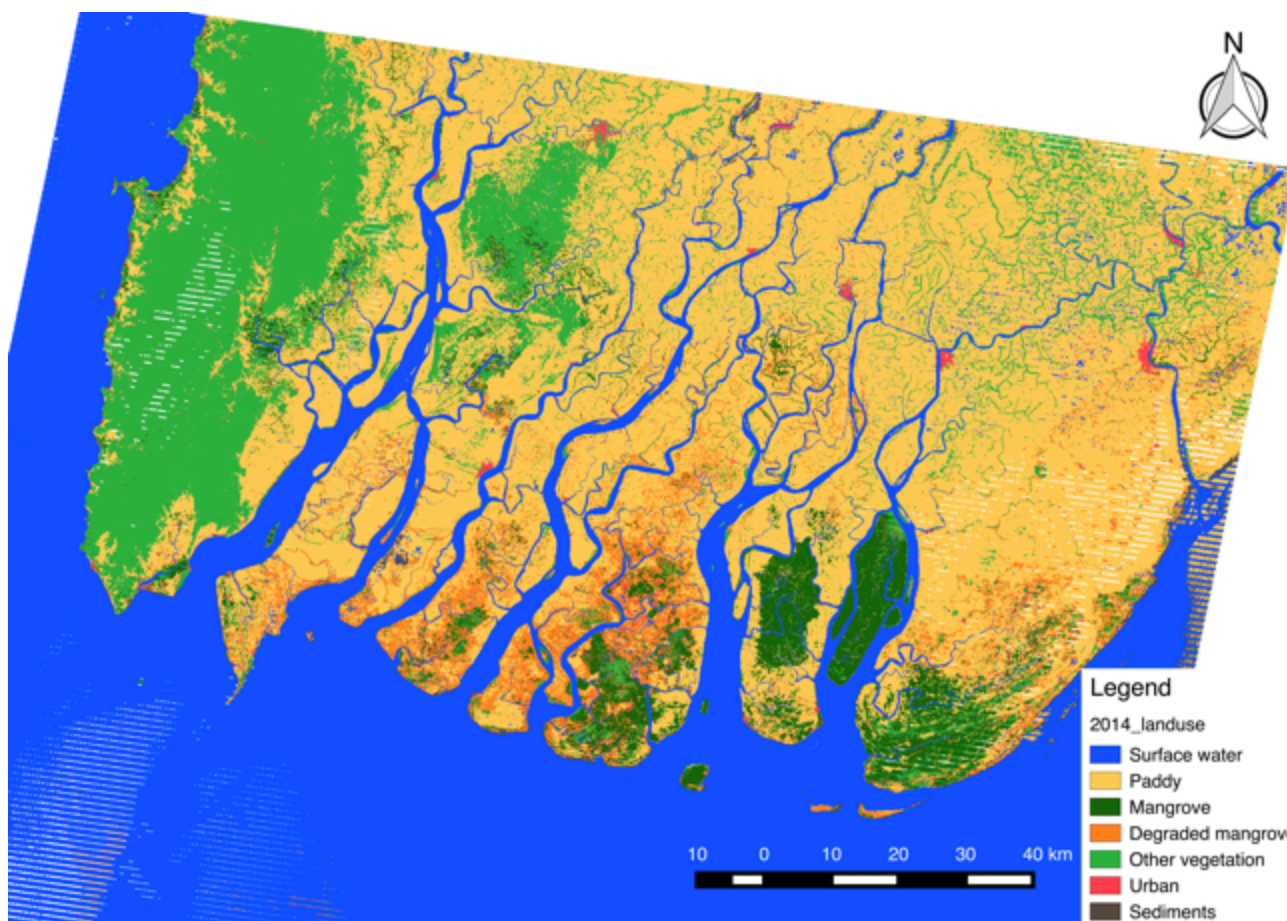


Figure 8. Classification of the merged 2014 image

Table 4. Hindcast of land use areas

Areas in sq. km.	1989	2000	2005	2008BN	2008AN	2010	2014
Surface water	5592.21	5790.48	6219.36	5779.22	5777.61	5912.94	5877.07
Paddy	5457.04	6021.75	4661.79	6161.27	6222.89	4649.31	4844.19

Mangrove	1129.62	692.96	654.51	119.03	310.32	480.91	837.52
Degraded mangrove	67.71	195.56	785.48	525.26	256.36	178.38	930.94
Other vegetation	2577.47	2343.86	2650.24	1851.71	2318.85	2852.7	2493.58
Urban	124.04	27	143.67	361.82	271	1052.59	144.56
Sediments	260.65	137.13	203.53	443.45	161.56	114.94	120.22
Other water body	5592.21	5790.48	6219.36	5779.22	5777.61	5912.94	5877.07
Total area	15208.74	15208.74	15318.58	15241.76	15318.59	15241.77	15248.08

3.2 Coastline position change

When coastlines extracted from satellite imagery between 1974 and 2014 are overlaid, the coastline does not show one overall trend of erosion or accretion. There are hotspots that can be identified, where accretion or erosion has occurred of more than 10 m/year on average (resulting in a total of 400 meters or more).

The overall coastline position between 1974 and 2014 is presented in Figure 9, and a more detailed map for two hotspots in Figure 10.

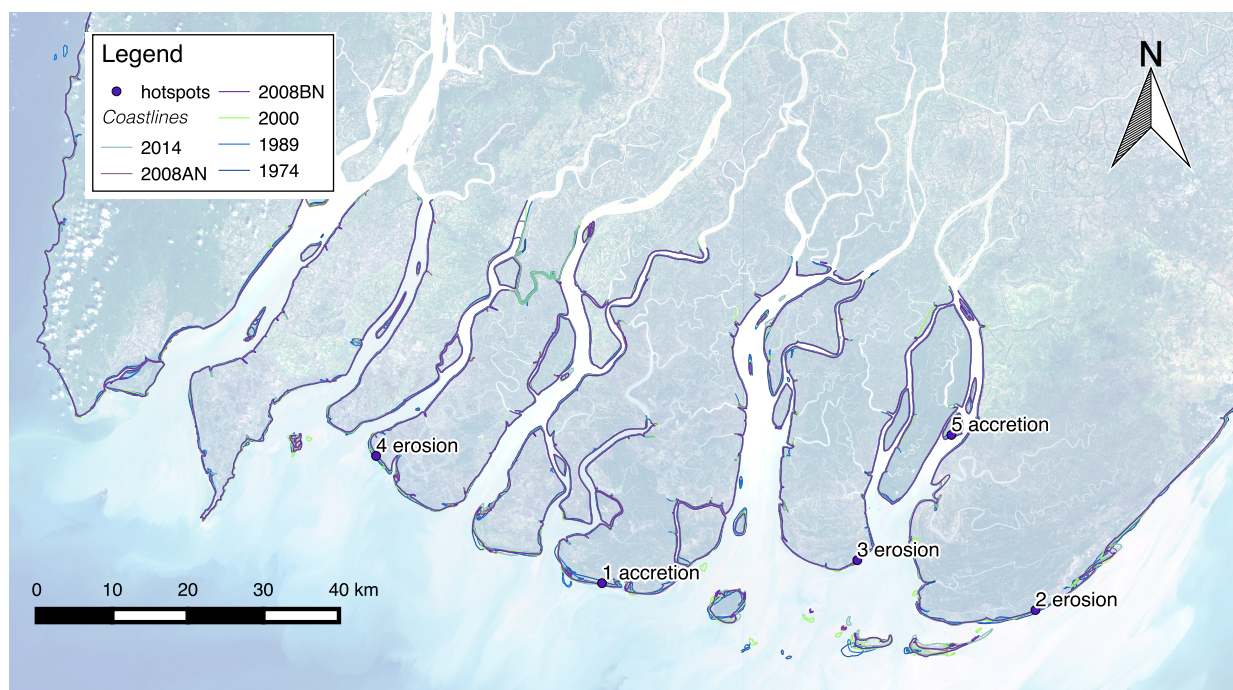


Figure 9. Coastline position between 1974 – 2014, with indicated hotspots

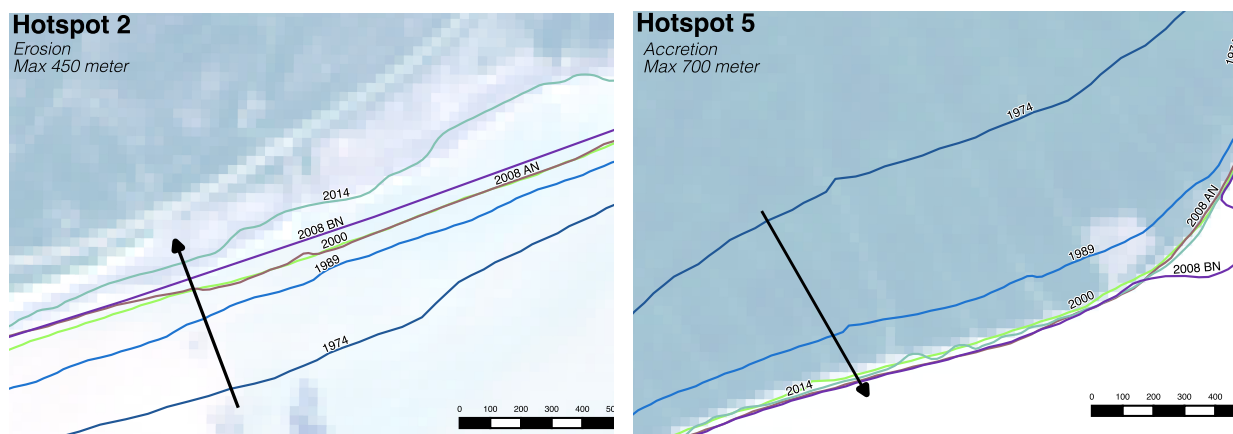


Figure 10. Two hotspots for coastline accretion or erosion

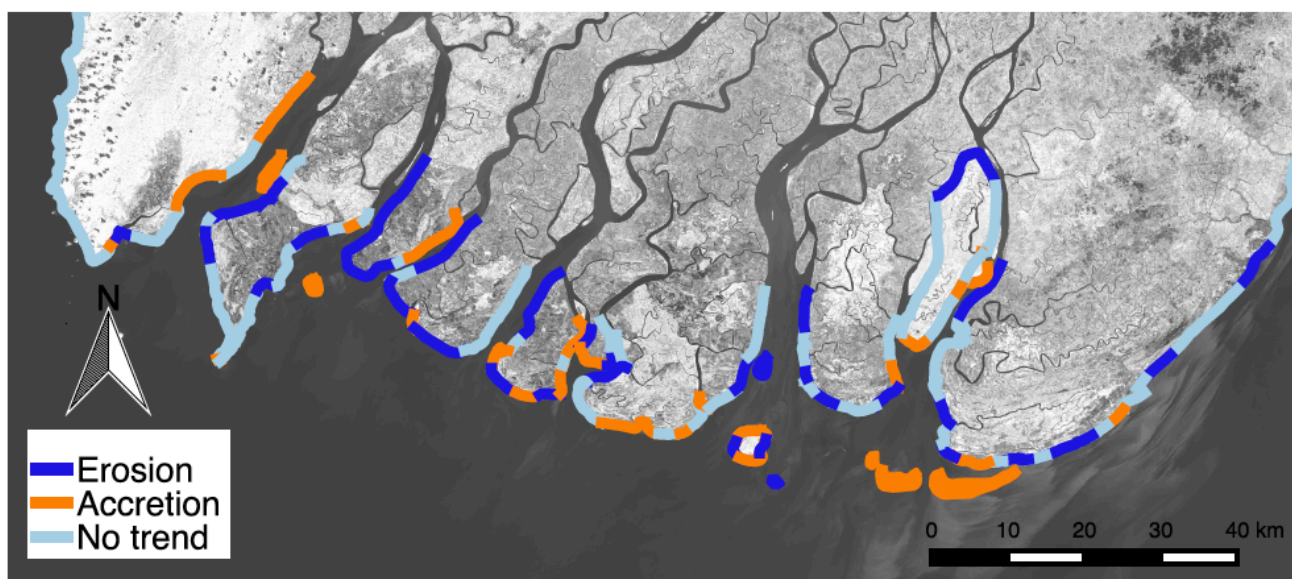


Figure 11. General overview of erosion/accretion along coastline between 1974 and 2014

4. DISCUSSION

In this research the land use has been classified and determined for the Ayeyarwady delta for seven satellite images between 1989 and 2014 and the position and dynamics of the coastline over the last 40 years has been identified. The coupling of coastline position and land use change could not be made based on this research due to various complications in the land use classification. Although there are several indicators which suggest the occurrence of coastal squeeze in the Ayeyarwady Delta, based on the results presented in this paper it cannot be proven whether it is occurring or not. In the next sections we will provide some recommendations on improvements that can be made on the methodology, for future research on this topic.

4.1 Land use classification

The training data and the classification method used proved to be sufficient to classify the land uses in the 2014 image. For the hindcast of land use on older satellite images, the areas of land use were fluctuating too much in order to trust their validity. We expect that the following factors are causing this:

First of all, the accuracy of the land use classification is highly dependent on the quality of the Landsat images. A lot of images contain clouds (and their shadows). The influenced pixels cannot be used for classification, and hence have to be patched with pixels from other images. Landsat 7 images after 2003 have large data gaps (22% of the total image) due to the breakdown of the SLR, which have to be patched as well. Patching of images results in differences in pixel values among the same types of land use. Also, Landsat images are originally provided in DN (digital number) format, and in order to compare the images they have to be radiometrically corrected (i.e. atmospheric correction and calibration to surface reflectance values). USGS has its own algorithm sequence for this, and the Landsat CDR database provides these 'ready-made' surface reflectance images. However, the reflectance of the same type of land cover was not the same on images captured on different dates. Therefore the Landsat CDR was histogram matched, which then again distorts the actual physical meaning of the reflectance values. Pons et al (2014) propose a new method to perform radiometric correction, and they claim this method provides better results than the Landsat CDR images. Applying the technique of Pons et al (2014) might result in a more accurate land use classification.

Furthermore, Nagol et al (2014) investigated bidirectional effects (effects of sun-target-sensor geometry) in Landsat images. They concluded that these effects are prevalent in Landsat images, and even small variations in viewing and illumination geometry have large impacts on the values of reflectance (mainly in the red and Near Infrared bands) and vegetation indices, especially near the equator. I.e., this affects the Landsat images we have used for this research. Correcting for bidirectional effects might increase the precision of our Landsat land use classification.

As the paddy growth-cycles are short, the spectral signatures of a paddy field can differ a lot. Also, even though the Landsat images that were used were taken around the same time of year, the weather conditions could have been different that year (colder/hotter or dryer/wetter than average), which has an influence on the vegetation. Therefore the process of signature extension might also improve the quality of the classifications. It requires a training dataset which contains a relatively small number of land cover observations that is spatially and temporally distributed (Sexton et al, 2013). In this research only a spatially distributed training data set was used. Expanding the training data set, both spatially and temporally, might also increase the accuracy.

Finally, the quality of the land use maps can also be improved by developing a multi sensor product, combining LandSat with Sentinel-1 radar (which is not affected by clouds and can also measure subsidence), MODIS, or IKONOS (which have a higher spatial resolution compared to Landsat).

4.2 Coastline position

For reliable forecasting of coastal evolution the period of 40 years, which can be drawn up from the Landsat imagery, is too short (Stive et al, 2002). Therefore an attempt was made to couple this to coastlines extracted from older analogue maps. When these results are combined it shows that the accuracy of these maps is not comparable with the satellite imagery, which can be seen in Figure 12. Difference in coastlines from maps (1941 and 1950) and satellite imagery is too large to be used for analysis. Furthermore georeferencing very old maps (<1800) proved to be challenging because of the absence of reliable referencing points. There is still a lot of quantitative and qualitative knowledge to be gained about this dynamic coastal environment and on the methods that can help with early recognition of coastal squeeze.

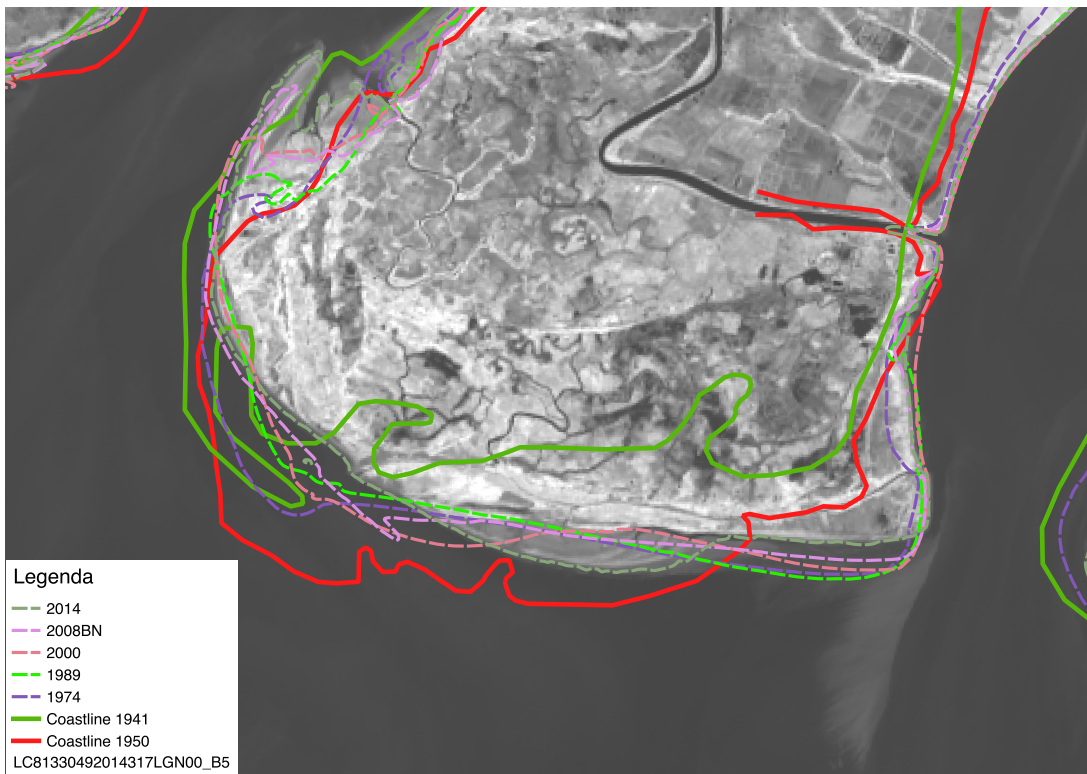


Figure 12. Difference in coastlines from maps (1941 and 1950) and satellite imagery

5. REFERENCES

Aung, Hla Tun, Myanmar: the study of processes and patterns, National Centre for Human Resource Development, Publishing Committee, Ministry of Education (2003)

H. L. Chhibber, and R. Ramamirtham, The geology of Burma, Macmillan, (1934)
ISO 690

J. P. Doody, 'coastal squeeze'— a historical perspective, *Journal of Coastal Conservation* 10, 129 (2004).

H. M. Fritz, C. D. Blount, S. Thwin, M. K. Thu, and N. Chan, Cyclone nargis storm surge in myanmar, *Nature Geoscience* 2, 448 (2009).

T. Furuichi, Z. Win, and R. Wasson, Discharge and suspended sediment transport in the Ayeyarwady river, Myanmar: centennial and decadal changes, *Hydrological processes* 23, 1631 (2009).

P. J. Hedley, M. I. Bird, and R. A. Robinson, Evolution of the irrawaddy delta region since 1850, *The Geographical Journal* 176, 138 (2010).

M. Kass, A. Witkin, and D. Terzopoulos, Snakes: Active contour models. *International journal of computer vision*, 1(4), 321-331(1988)

J. R. Nagol, J. O. Sexton, D.H. Kim, A. Anand, D. Morton, E. Vermote, and J. R. Townshend, Bidirectional effects in landsat reflectance estimates: Is there a problem to solve? *ISPRS Journal of Photogrammetry and Remote Sensing* (2014).

- L. K. Phan, J. S. M. van Thiel de Vries, M. J. F. Stive, Coastal Mangrove Squeeze in the Mekong Delta, *Journal of Coastal Research* (unpublished) (2014)
- X. Pons, L. Pesquer, J. Cristóbal, and O. González-Guerrero, Automatic and improved radiometric correction of landsat imagery using reference values from MODIS surface reflectance images, *International Journal of Applied Earth Observation and Geoinformation* 33, 243 (2014).
- P. Rao, V. Ramaswamy, and S. Thwin, Sediment texture, distribution and transport on the ayeyarwady continental shelf, andaman sea, *Marine geology* 216, 239 (2005).
- K. S. Rodolfo, The Irrawaddy delta: tertiary setting and modern offshore sedimentation, (1975). Chhibber, Harbans Lal, and R. Ramamirtham. *The geology of Burma*. Macmillan, 1934.
- D. P. Roy, J. Ju, K. Kline, P. L. Scaramuzza, V. Kovalskyy, M. Hansen, T. R. Loveland, E. Vermote, and C. Zhang, Web-enabled landsat data (weld): Landsat etm+ composited mosaics of the conterminous united states, *Remote Sensing of Environment* 114, 35 (2010).
- J. O. Sexton, D. L. Urban, M. J. Donohue, and C. Song, Long-term land cover dynamics by multi-temporal classification across the landsat-5 record, *Remote Sensing of Environment* 128, 246 (2013).
- M. J. Stive, S. G. Aarninkhof, L. Hamm, H. Hanson, M. Larson, K. M. Wijnberg, R. J. Nicholls, and M. Capobianco, Variability of shore and shoreline evolution, *Coastal Engineering* 47, 211 (2002).
- D. Walling, Human impact on land–ocean sediment transfer by the world’s rivers, *Geomorphology* 79, 192 (2006).
- R. E. Waterman, "Integrated coastal policy via Building with Nature." *Oceanographic Literature Review* 42.12 (1995) .
- E. L. Webb, N. R. Jachowski, J. Phelps, D. A. Friess, M. M. Than, and A. D. Ziegler, Deforestation in the ayeyarwady delta and the conservation implications of an internationally-engaged Myanmar, *Global Environmental Change* 24, 321 (2014).
- S. J. Weber, L. Keddell, and M. Kemal, Myanmar ecological forecasting: Utilizing nasa earth observations to monitor, map, and analyze mangrove forests in myanmar for enhanced conservation (2014).
- Republic of the Union of Myanmar “The Population and Housing Census of Myanmar, 2014 – Summary of the Provisional Results” (2014) Accessed through http://unstats.un.org/unsd/demographic/sources/census/2010_phc/Myanmar/MMR-2014-08-28-provres.pdf - on 29-01-2015